Proceedings of the Third International Conference on Inventive Systems and Control (ICISC 2019)
DVD Part Number: CFP19J06-DVD; ISBN: 978-1-5386-3949-8

EKF and UKF for estimating the liquid level inside gas-liquid cylindrical cyclone

Mishiga Vallabhan*, Torstein Thode Kristoffersen† and Christian Holden‡
Department of Mechanical and Industrial Engineering,
Norwegian University of Science and Technology (NTNU)
Email: *mishiga.vallabhan@ntnu.no, †torstein.t.kristoffersen@ntnu.no, ‡christian.holden@ntnu.no

***Abstract*—The oil and gas industry is focussing more on subsea separation and processing and the need for compact equipment such as gas-liquid cylindrical cyclones (GLCC) is increasing. As compactness of the equipment increases, they become more sensitive to variations in the input conditions and the dynamics become faster. Improving the control aspect is one of the solutions to ensure efficient operation of these devices during all field conditions. However, the measurements available are limited due to higher instrument cost or the absence of proper sensors. Virtual sensors or estimators is an alternative technology which could solve the problem with lower investment cost. In the case of gas-liquid cylindrical cyclones, there is no proper sensor to measure the level inside it. Therefore, this paper focuses on estimating the level inside a GLCC using two well-know nonlinear estimation techniques, the EKF and the UKF. The estimates are given as a state feedback to a level controller.**

I. Introduction

Gas-liquid cylindrical cyclones (GLCC) are considered as an alternative to conventional gravity-based separators in the oil and gas industry [1]. A mixture of gas and liquid (from the reservoir) enters the GLCC through a tangential inlet, which creates a swirl in the flow. The liquid moves to the side due to the centrifugal forces induced by the swirling effects, while the gas accumulates in the center due to density differences. Gravity also pulls the liquid down while the gas rises. Simple, compact and low operational costs makes GLCCs attractive for various applications such as multiphase flow metering, pre-separation of raw gas from high pressure wells [2] and as a compact separator in subsea applications.

In cases were GLCC is used as a separator liquid level and pressure control are required to reduce gas carry under (GCU) into the liquid stream and liquid carry over (LCO) into the gas stream. The pressure at the gas outlet is measured and given as feedback to the pressure control loop. The complex hydrodynamic nature of flow inside the GLCC makes the level measurement inaccurate, but the equilibrium liquid level can be measured [2] and given as a feedback to the level control loop. However, the fast dynamics of a GLCC renders such a measurement insufficient.

In [3], a dynamic model with perfect separation controlled by a PI feedback controllers was presented, and [4] extended it with a gain-scheduling controller. Later, [5] proposed an empirical dynamic model with imperfect separation and a feedforward algorithm. Recently, [6] derived a control-oriented model of a GLCC with separation dynamics of the inlet gas-liquid flow and [7] extended the model by considering the continuous separation of gas and liquid phase.

As mathematical models, in particular state space models, open up the possibility of using estimators for estimating parameters and unmeasured states, [8] has used an extended Kalman filter (EKF) for paramater estimation of a GLCC assuming full state knowledge, and [9] applied an unscented Kalman filter (UKF) and linear moving horizon estimator (MHE) for state and parameter estimation of the GLCC assuming limited-state knowledge. Both [8] and [9] assumed that level measurements were available; however as mentioned earlier, the level is difficult to measure. In this paper, we are focussing on estimating the level using other available measurements (gas outlet pressure, mass flow rates and densities). A nonlinear GLCC model developed in [7] is used as a plant model and a simplified estimator model is derived by a state transformation. Owing to the nonlinearity in the model we are using two nonlinear estimators: a EKF and a UKF.

The EKF is a common choice for nonlinear estimator problems despite being based on first order linearization. The EKF is an extension of the Kalman filter, with an additional step of calculating the Jacobian matrices which linearizes the nonlinear dynamics. Calculation of the Jacobians is difficult in higher order systems, and a well known drawback is that the linearization can introduce errors in the system which may later cause the estimates to diverge.

The UKF is another technique for nonlinear estimator problems. The UKF is an improvement of the EKF and creates sample points (sigma points) around the current state estimate based on the covariance. Each of these sample points are transformed through the nonlinear dynamics and used to calculate the new mean and error covariance. The GLCC is an integrating process, and is highly unstable without the level and the pressure control. In our analysis we have considered the level and the pressure as controlled by independent controllers and the estimates are given to these controllers.

II. GLCC model

The GLCC plant model used in this paper is adopted from [7], where dynamic mass balances are combined with online steady-state separation calculations of liquid carry over (LCO) at the gas outlet stream and gas carry under (GCU) at the liquid outlet stream of the GLCC. As complete separation is not possible, the inlet gas-liquid flow entering the GLCC is

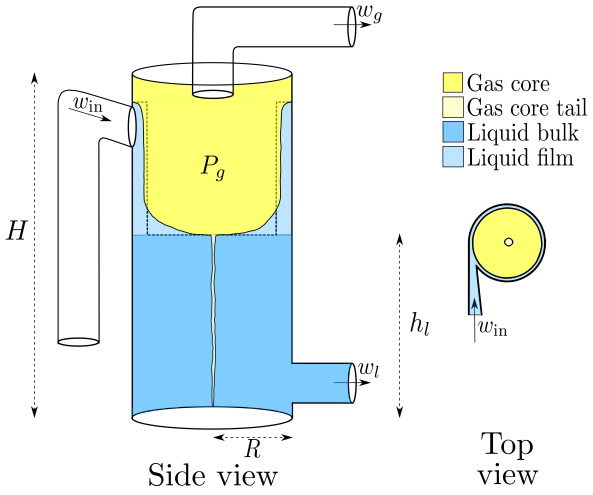

Fig. 1. A sketch of a gas-liquid cylindrical cyclone showing gas-liquid interface [6]

separated as a gas stream containing liquid droplets and a liquid stream containing gas bubbles. Hence, there are four mass balances describing the system states of the GLCC: gas and liquid in the predominantly liquid volume, and gas and liquid in the predominantly gas volume:

$$\dot{m}_{l,l} = w_{in,l} - w_{lco} - w_{l,l} \tag{1}$$
$$\dot{m}_{l,g} = w_{gcu} - w_{l,g} \tag{2}$$
$$\dot{m}_{g,l} = w_{lco} - w_{g,l} \tag{3}$$
$$\dot{m}_{g,g} = w_{in,g} - w_{gcu} - w_{g,g} \tag{4}$$

where $m_{l,l}$ is the mass of liquid in the liquid volume, $m_{l,g}$ is the mass of gas in the liquid volume, $m_{g,l}$ is the mass of liquid in the gas volume, $m_{g,g}$ is the mass of liquid in gas volume, $w_{in,l}$ and $w_{in,g}$ are liquid and gas flow components in the inlet flow w_{in}, $w_{l,l}$ and $w_{l,g}$ are liquid and gas components in liquid outlet stream w_l, $w_{g,l}$ and $w_{g,g}$ are liquid and gas outlet components in the gas outlet stream w_g, w_{gcu} is the GCU mass flow and w_{lco} is the LCO mass flow.

The inlet gas mass fraction $\beta_{in} \in [0,1]$ is defined as

$$\beta_{in} \triangleq \frac{m_{in,g}}{m_{in,l} + w_{m,g}} , \tag{5}$$

where $m_{in,g}$ is the mass of gas in the inlet stream and $m_{in,l}$ is the mass of liquid in the inlet stream. The liquid and gas mass flows in the model are expressed in terms of gas mass fraction. The inlet mass flows of liquid and gas are given by

$$w_{in,g} = \beta_{in} w_{in} \tag{6}$$
$$w_{in,l} = (1 - \beta_{in}) w_{in} . \tag{7}$$

In this model, LCO and GCU are modelled based on the separation factors $\epsilon_{LCO} \in [0,1]$ and $\epsilon_{GCU} \in [0,1]$

$$w_{lco} = \epsilon_{LCO}(1 - \beta_{in}) w_{in} \tag{8}$$
$$w_{gcu} = \epsilon_{GCU} \beta_{in} w_{in} . \tag{9}$$

We can rewrite the mass balance equations as

$$\dot{m}_{l,l} = (1 - \epsilon_{LCO})(1 - \beta_{in}) w_{in} - w_{l,l} \tag{10}$$
$$\dot{m}_{l,g} = \epsilon_{GCU} \beta_{in} w_{in} - w_{l,g} \tag{11}$$
$$\dot{m}_{g,l} = \epsilon_{LCO}(1 - \beta_{in}) w_{in} - w_{g,l} \tag{12}$$
$$\dot{m}_{g,g} = (1 - \epsilon_{GCU}) \beta_{in} w_{in} - w_{g,g} . \tag{13}$$

Though the GLCC model described by (10)–(13) does not appear complicated, calculations of the separation factors ϵ_{LCO} and ϵ_{GCU} based on the droplet and bubble trajectories are highly complex and non-linear. The equations describing the separation factors are given in [6]. We also consider the two control valves (Fig. 2) as part of the plant model and the flow through the valve are modelled as

$$w_l = C_{dl} A_{vl} u_l \sqrt{\rho_l (P_l - P_{lb})} \tag{14}$$
$$w_g = C_{dg} A_{vg} u_g \sqrt{\rho_g (P_g - P_{gb})} . \tag{15}$$

where C_{dl} and C_{dg} are the valve constants of the level and the pressure control valve, A_{vl} and A_{vg} are the cross-sectional areas of the level and the pressure control valves, u_l and $u_g \in [0,1]$ are the level and pressure control signals, and P_{lb} and P_{gb} are the back pressures at liquid and gas outlets. The model assumes that these two back pressures are known. P_l and P_g are the pressures at the liquid and gas outlets.

III. Estimator Modelling

The plant model described by (10)–(13) is complex to be implemented as an estimator model. Hence we simplify this model and introduce two variables m_l and m_g, respresenting total mass flow in the liquid and gas outlet of the GLCC, respectively, giving

$$m_l = m_{l,l} + m_{l,g} \tag{16}$$
$$m_g = m_{g,l} + m_{g,g} . \tag{17}$$

Then, from (10)–(13), we get

$$\dot{m}_l = [(1-\beta_{in}) - \epsilon_{LCO}(1 - \beta_{in}) + \epsilon_{GCU}\beta_{in}] w_{in} - w_l \tag{18}$$
$$\dot{m}_g = [\beta_{in} - \epsilon_{GCU}\beta_{in} + \epsilon_{LCU}(1 - \beta_{in})] w_{in} - w_g . \tag{19}$$

The further derivation is based on the following assumptions:

1) The density of the light liquid volume is assumed to be approximately equal to that of pure liquid.
2) The amount of liquid droplets in the gas volume is small and neglected for the calculation of pressure.
3) The liquid level inside the GLCC is assumed to be flat, but in reality the level is curved and disturbed by the inlet flow and the gas bubbles. Fig. 1 shows the gas-liquid interface inside the GLCC.

The height h_l of the liquid column in the GLCC is given by

$$h_l = \frac{m_l}{\rho_l A} \tag{20}$$

where A is the cross sectional area of GLCC and ρ_l is the liquid density. The rate of change $\dot{h_l}$ is given by

$$\begin{aligned}\dot{h_l} &= \frac{\dot{m_l}}{\rho_l A} \\ &= \frac{[(1-\beta_{in})-\epsilon_{LCO}(1-\beta_{in})+\epsilon_{GCU}\beta_{in}]w_{in}-w_l}{\rho_l A} .\end{aligned} \tag{21}$$

The ideal gas law gives the pressure P_g at the gas outlet stream

$$P_g V_g = \frac{m_g}{M_g} RT , \tag{22}$$

where M_g is the molar mass of clean gas, R is the ideal gas constant and T is the temperature. Time differentiation gives

$$\frac{dP_g}{dt} V_g + \frac{dV_g}{dt} P = \frac{RT}{M_g} \dot{m}_g . \tag{23}$$

Knowing that $V = V_l + V_g$ and $\dot{V} = 0$ implies $\dot{V_l} = -\dot{V_g} = A\dot{h_l}$. Applying this and inserting (19) and (21) yields

$$\begin{aligned}\frac{dP_g}{dt}(V - V_l) - \frac{dV_l}{dt} P_g &= \frac{RT}{M_g}\dot{m}_g \\ \dot{P_g}(V - V_l) - \frac{A dh_l}{dt} P_g &= \frac{RT}{M_g}\dot{m}_g \\ \dot{P_g} = \frac{1}{A(H-h_l)} \Bigg[&\frac{RT}{M_g}([\beta_{in} - \epsilon_{GCU}\beta_{in} + \\ \epsilon_{LCU}(1-\beta_{in})]w_{in} - w_g) &+ \frac{P_g}{\rho_l}[(1-\beta_{in}) - \\ \epsilon_{LCO}(1-\beta_{in}) + \epsilon_{GCU}\beta_{in}]w_{in} - w_l \Bigg]\end{aligned} \tag{24, 25}$$

where H is the total height of the GLCC.

For use in the estimator, we simplify the model further. The inflow w_{in}, which is a mixture of gas and liquid, is split into two outflows w_l and w_g. By inserting a split factor α describing the separation ratio of gas and liquid at two outlets given by

$$w_g = \alpha w_{in} \tag{26}$$

$$w_l = (1-\alpha) w_{in} . \tag{27}$$

The mass flow rate at the liquid outlet can be expressed as

$$\frac{dm_l}{dt} = \alpha w_{in} - w_l . \tag{28}$$

Assuming that the density ρ_l remains constant gives

$$\frac{dh_l}{dt} = \frac{\alpha w_{in} - w_l}{A\rho_l} . \tag{29}$$

The rate of change of accumulated mass of gas is given by

$$\frac{dm_g}{dt} = (1-\alpha) w_{in} - w_g . \tag{30}$$

The gas pressure is given by the ideal gas law (22)

$$m_g = \frac{P_g V_g M_g}{RT} . \tag{31}$$

Inserting (30) into (31) gives

$$\begin{aligned}\frac{d}{dt}\left(\frac{P_g V_g M_g}{RT}\right) &= (1-\alpha) w_{in} - w_g \\ \frac{M_g}{RT}\left[\frac{dP_g}{dt} V_g + \frac{dV_g}{dt} P_g\right] &= (1-\alpha) w_{in} - w_g \\ \frac{M_g}{RT}\left[\frac{dP_g}{dt} A(H-h_l) - \frac{dV_l}{dt} P_g\right] &= (1-\alpha) w_{in} - w_g .\end{aligned} \tag{32}$$

Since $\dot{V_l} = A\dot{h_l}$, using (29) gives

$$\frac{M_g}{RT}\left[\frac{dP_g}{dt} A(H-h_l) - \frac{P_g}{\rho_l}(\alpha w_{in} - w_l)\right] = (1-\alpha) w_{in} - w_g . \tag{33}$$

Rearranging the terms gives,

$$\frac{dP_g}{dt} = \frac{\frac{RT}{M_g}((1-\alpha) w_{in} - w_g) + \frac{P_g}{\rho_l}(\alpha w_{in} - w_l)}{A(H-h_l)} . \tag{34}$$

To summarise and make the estimator equation distinguishable from the plant model, (29) and (34) are appended with estimator notation and are written as

$$\dot{\hat{h}}_l = \frac{\alpha w_{in} - w_l}{A\rho_l} \tag{35}$$

$$\dot{\hat{P}}_g = \frac{\frac{RT}{M_g}((1-\alpha) w_{in} - w_g) + \frac{\hat{P}_g}{\rho_l}(\alpha w_{in} - w_l)}{A(H-\hat{h}_l)} . \tag{36}$$

Comparing equations (21), (25), (35) and (36), the split factor α is algebraically mapped to the separation factors and the inlet gas mass fraction as

$$\alpha = (1-\beta_{in}) - \epsilon_{LCO}(1-\beta_{in}) + \epsilon_{GCU}\beta_{in} \tag{37}$$

$$(1-\alpha) = \beta_{in} - \epsilon_{GCU}\beta_{in} + \epsilon_{LCU}(1-\beta_{in}) . \tag{38}$$

The state-space representation of the estimator model is then given as

$$\dot{x}_1 = \frac{x_3 w_{in} - w_l}{A\rho_l} \tag{39}$$

$$\dot{x}_2 = \frac{c\left[\frac{RT}{M_g}((1-x_3) w_{in} - w_g) + \frac{x_2}{\rho_l}(x_3 w_{in} - w_l)\right]}{A(H-x_1)} \tag{40}$$

$$\dot{x}_3 = \frac{-x_3}{\mathcal{T}} , \tag{41}$$

The variable x_1 [m] is the height of liquid column inside the GLCC, x_2 [bar] is the gas outlet pressure and x_3 [-] is the split factor which we model by a Wiener filter with $\mathcal{T}$ time constant The measurement model of the GLCC is given by

$$z = [0, x_2, x_3]^T . \tag{42}$$

IV. EKF Design

As the model is nonlinear, we are using the nonlinear extension of the Kalman filter for estimating the system states. The two main extensions of the Kalman filters are the linearized Kalman filter (LKF) and the EKF [10, Ch. 13].

The LKF linearizes the nonlinear system around some nominal state trajectory that is not updated based on the

measurements. While the EKF, linearizes the nonlinear system around the current estimates. In other words, EKF linearizes the nonlinear system around the current Kalman filter estimate. Here we are using the EKF, specifically the continuous-time EKF as the plant and the estimator model are in continuous time. The general formation of continuous time EKF is presented below [10, Ch. 13], Consider a estimator model,

$$\dot{x} = f(x,u) + W \tag{43}$$
$$z = h(x) + V \ , \tag{44}$$

where W is the process noise and V is the measurement noise with distributions $\mathcal{N}(0,Q)$ and $\mathcal{N}(0,R)$, respectively, and f is derived from (39)–(41). The first step of the EKF is to initialise the filter

$$\begin{aligned} \hat{x}(0) &= E[x(0)] \\ P(0) &= E[(x(0)-\hat{x}(0))(x(0)-\hat{x}(0))^T] \ . \end{aligned} \tag{45}$$

The next step of the EKF is to compute the Jacobians for the process and measurement models at the current state estimate (at $t=0$ the Jacobians are calculated at the initial value)

$$F = \left.\frac{\partial f}{\partial t}\right|_{\hat{x}} \tag{46}$$
$$H = \left.\frac{\partial h}{\partial t}\right|_{\hat{x}} \ . \tag{47}$$

As the continuous-time EKF combines the prediction and update steps of the ordinary Kalman filter, the final update step is given as

$$\dot{\hat{x}} = f(\hat{x},u) + K[z - h(\hat{x})] \tag{48}$$
$$\dot{P} = FP + PF^T - KHP + Q \tag{49}$$
$$K = PH^T R^{-1} \tag{50}$$

The performance of the EKF depends heavily on tuning of the covariance matrices for the process and measurement noises. The tuning of Q and R have large impact on plant-model mismatch.

A trial-and-error-based approach was used for tuning of Q and R. The covariance matrices were selected to reduce the estimation errors of the two states x_2 and x_3 (pressure and split factor), which have direct measurements from sensors. As the estimation of x_2 and x_3 approached the actual value, x_1 moves away from the actual value. This could be because of plant-model mismatch or due to the EKF method itself. A biased estimate of x_2 and x_3 gave a better estimate of x_1. As the main focus of the estimation is to get the level (unmeasured) closer to the actual value, the other two estimates were penalised. The covariance matrix used in simulation are listed in Table I.

TABLE I
TUNING PARAMETERS

Q_{EKF}	$\text{diag}([1\times10^{-8}, \quad 2.5\times10^{-}3, \quad 2304])$
R_{EKF}	$\text{diag}([10, \quad 0.6])$
Q_{UKF}	$\text{diag}([3.564\times10^{-}5, \quad 2.5\times10^{-}3, \quad 900])$
R_{UKF}	$\text{diag}([0.005, \quad 1])$

V. UKF DESIGN

The UKF is a Gaussian sampling method that chooses sampling points (or sigma points) based on a deterministic approach.

For a vector x, with mean $\bar{x}$ and covariance P_x, then with the unscented transform [11], [12], a set of samples are deterministically selected from the probability distribution of x, i.e., if x is an $n\times1$ vector we choose $2n$ sigma points $X_{(i)}$ as

$$X_{(i)} = \begin{cases} \bar{x} + (\sqrt{nP_x})_i^T, & i = 1,...,n \\ \bar{x} - (\sqrt{nP_x})_i^T, & i = n+1,...,2n, \end{cases} \tag{51}$$

where $\sqrt{nP_x}$ is the matrix square root of nP such that $(\sqrt{nP_x})^T\sqrt{nP_x} = nP_x$ (since P is positive definite) and $(\sqrt{nP_x})_i$ is the ith row $\sqrt{nP_x}$. Consider the nonlinear transformation $y = f(x)$, then each of these sigma points are transformed through this nonlinear transformation to get a corresponding set of sample points in $Y_{(i)} = f(X_{(i)})$. Now, we can derive the estimates of the mean and covariance of y as

$$\begin{aligned} \bar{y} &= \frac{1}{2n}\sum_{i=1}^{2n} Y_{(i)} \\ P_y &= \frac{1}{2n}\sum_{i=1}^{2n}(Y_{(i)} - y_u)(Y_{(i)} - y_u)^T \end{aligned} \tag{52}$$

The unscented transformation described above is used in the UKF to estimate the state and the error covariance. Consider the discrete-time nonlinear system with process and measurement model,

$$x_{k+1} = f_d(x_k, u_k) + W_k \tag{53}$$
$$z_k = h(x_k) + V_k \tag{54}$$

where $W_k \sim \mathcal{N}(0,Q_k)$ and $V_k \sim \mathcal{N}(0,Q_k)$ are additive process and measurement noise, and f_d is the discretised version of (43). The UKF algorithm consist of the following steps:

- Initialise UKF at $k=0$

$$\hat{x}_0 = E[x_0], \hat{P}_0 = E[(x_0 - \hat{x_0})(x_0 - \hat{x_0})^T] \ . \tag{55}$$

- Choose the samples or sigma points based on the current state and covariance:

$$X_{k-1} = [\hat{x}_{k-1} + \sqrt{nP_{k-1}} \quad \hat{x}_{k-1} - \sqrt{nP_{k-1}}] \tag{56}$$

- The prediction step in the UKF is given by transforming the set of sigma points individually through the nonlinear function f:

$$X_k^{(i)-} = f(X_{k-1}^{(i)-}, u_k) \ . \tag{57}$$

Then recreate the a priori state estimate and its error covariance

$$\hat{x}_k^- = \frac{1}{2n}\sum_{i=1}^{2n} X_k^{(i)-}$$
$$P_k^- = \frac{1}{2n}\sum_{i=1}^{2n}(X_k^{(i)-} - \hat{x}_k^-)(X_k^{(i)-} - \hat{x}_k^-)^T + Q_k \ . \tag{58}$$

- In the measurement update, we can use the new state estimate and its error covariance to re-sample new sigma points as

$$X_k^- = [\hat{x}_k^- + \sqrt{nP_k^-} \quad \hat{x}_k^- - \sqrt{nP_k^-}] \ . \tag{59}$$

To obtain the measurement update, the next step is to project the new sigma points through the measurement function h and evaluate covariance and cross covariance to compute the Kalman gain:

$$Z_k^{(i)-} = h(X_k^{(i)-}) \tag{60}$$
$$\hat{z}_k^- = \frac{1}{2n}\sum_{i=1}^{2n} Z_k^{(i)-} \tag{61}$$
$$(P_z^-)_k = \frac{1}{2n}\sum_{i=1}^{2n}(Z_k^{(i)-} - \hat{z}_k^-)(Z_k^{(i)-} - \hat{z}_k^-)^T + R_k \tag{62}$$
$$(P_{xz}^-)_k = \frac{1}{2n}\sum_{i=1}^{2n}(Z_k^{(i)-} - \hat{x}_k^-)(Z_k^{(i)-} - \hat{z}_k^-)^T \tag{63}$$
$$K_k = (P_{xz}^-)_k (P_z^-)_k^{-1} \tag{64}$$

- Update the state estimate and the error covariance using the Kalman gain:

$$\hat{x} = \hat{x}_k^- + K_k(z_k - \hat{z}_k^-) \tag{65}$$
$$P_k = P_k^- - K_k(P_z^-)_k K_k^T \tag{66}$$

The algorithm described above is taken from [10, Ch.14].

Another common type of UKF is to select $2n + 1$ sigma points and different weights for the state estimate and the covariance estimate [13]. The matrix version of UKF is given by [14], and this also gives derivation of the continuous time version of the UKF.

Another modification of the UKF is the constrained UKF [15], which is used if there are constraints on the states. This can increase the performance in these type of systems. E.g., "level cannot be negative" or "level cannot be higher than maximum tank capacity". In [16], methods for contraint handling in the EKF are described. One technique is the projection method, where the unconstrained state estimate $\hat{x}$ is projected onto the constrained boundary surface. In [15], this method is applied with a UKF; whenever the sigma points calculated during the time update is outside the feasible region, they are projected onto the feasible boundary region. The same procedure can be applied to sigma points calculated for the measurement update as well.

In this paper, we have implemented the constrained version of the UKF, since the unconstrained UKF was estimating negative values for the level, x_1. The constrain was imposed after transforming sigma points through the nonlinear function. Specifically, if there are any samples of x_1 taking a negative value after passing through the estimator model, then that sample is equated to 1 which is the lower constraint,

$$X_k^{(1)-} = \begin{cases} f(X_{k-1}^{(1)-}, u_k) & \text{if } X_k^{(1)-} > 1 \\ 1 & \text{otherwise} \ . \end{cases}$$

The lower limit of the constraint is tuned to reduce the bias in the estimate and the limit $X_k^{(1)-} = 1$ is found to a give better result than the physical limit $X_k^{(1)-} = 0$. These constrained sigma points are used later to recreate the a priori state estimate and its error covariance.

Note that the continuous-time version of the UKF has a combined prediction and upadte steps. In order to implement constraints after the prediction step we have chosen the discrete-time version of the UKF. The nonlinear discrete-time equivalent (39)–(41) is formulated using an RK4 integrator with time step equal to that of the simulation. The performance of the UKF also depends on the covariance matrices for the process and measurement noises. These were here chosen based on trial and error as, in Section IV. The final values used in the simulation is listed in Table I.

VI. Simulation

The simulation setup used for this paper is shown in Fig. 2. The plant is the full GLCC model (10)–(13) and two outlet control valves (14) and (15). The continuous separation model [7] for the GLCC is used in the simulation, as this is much closer to the real plant scenario. The pressure P_g and flow rates w_l and w_g are directly measured. The separation factor is derived by measuring the densities at the two outlets (a coriolis flowmeter could be an option in a real-life experiment). Separate PI feedback controllers are used to control the liquid level and the gas pressure. The tuning parameters for the controllers are the same as in [6]. The noisy measurements of P_g and α are given to the estimators and the output of the estimator, $\hat{\hat{h}}_l$ and $\hat{\hat{P}}_g$, are given to the controllers. The reference value of the level and the pressure is not changed during the simulation. Three different inlet flow conditions are applied by varying the inlet gas mass fraction flow as low, intermediate and high, as shown in Fig. 3. These input conditions are used in simulations for both UKF and EKF. The UKF and the EKF simulations vary only in which estimators were used; otherwise the same conditions were used in the simulations. For visualisation purpose the plots of the simulations are divided into 0–100 s (Figs. 4 and 6) and 100–900 s (Figs. 5 and 7).

Note that there is a bias in the estimated value in the EKF simulations and that the magnitude of the bias is smaller in the UKF simulations. The primary reason for this is plant-model mismatch. The simplified model is not be able to capture the right increases or decreases in inlet gas mass fraction. The

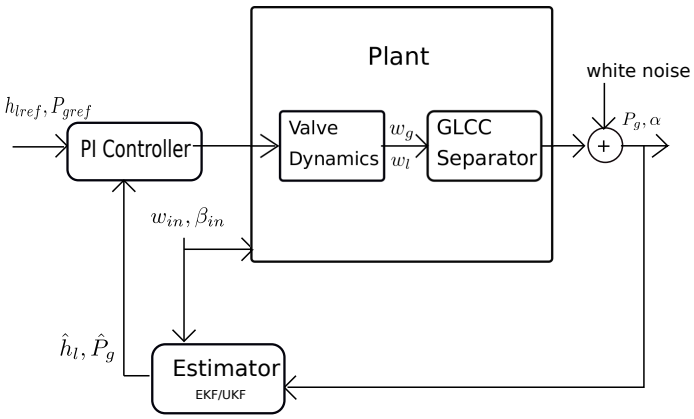

Fig. 2. Block diagram representation of plant estimator model.

TABLE II
RMS VALUES FOR THE ESTIMATOR

RMS	$x_1 - \hat{x}_1$	$x_2 - \hat{x}_2$
EKF	0.0331	0.0403
UKF	0.0067	0.0099

main aim of the simulations are to get the best estimate of the unmeasured state x_1. Both the EKF and the UKF are tuned in such a way that $\hat{x}_1$ is closer to x_1 at the expense of the estimate of the other two states. The EKF and the UKF is not that much effective in filtering out the noise in the separation factor α, however it is acceptable as we are not using it directly in the controller. In a real scenario, the pressure controller could directly use the measurement from the pressure sensor and the level controller could use the estimated value of h_l. The setpoint for the level controller is 1.5 m, and for the pressure controller 50 bar. All the parameters used for the simulation are listed in the Table III. The RMS values calculated for two estimates ($\hat{x}_1$ and $\hat{x}_2$) used in the controller are given in Table II. These values clearly indicate that the UKF gives better performance than the EKF.

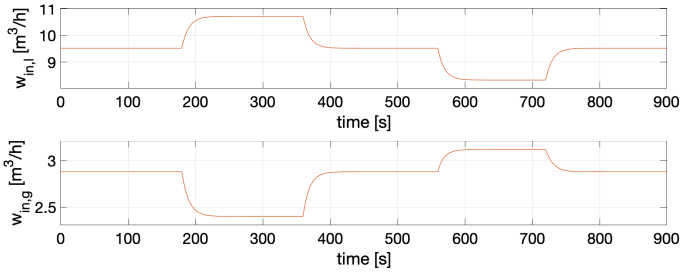

Fig. 3. Gas and the liquid inflow values during simulations.

VII. CONCLUSION

In this paper, we have compared two nonlinear Kalman filters (EKF and UKF) for estimating the unmeasured liquid level inside the gas-liquid cylindrical cyclone (GLCC). Estimates were fed to nominal level and pressure controlleres. Direct

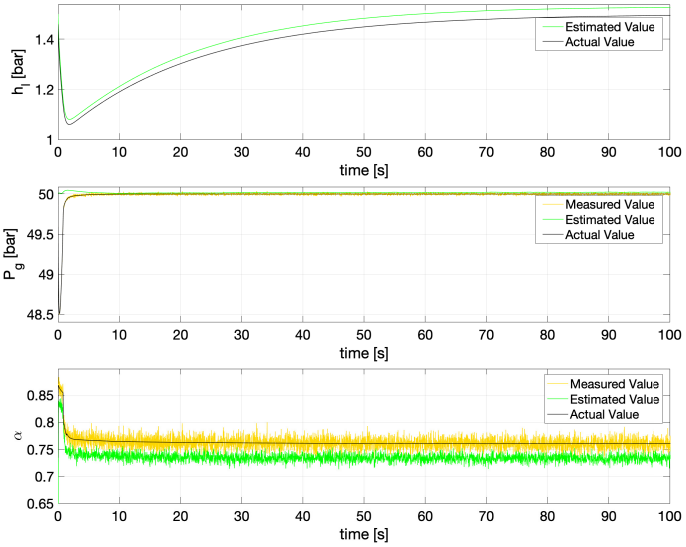

Fig. 4. EKF 0–100 s.

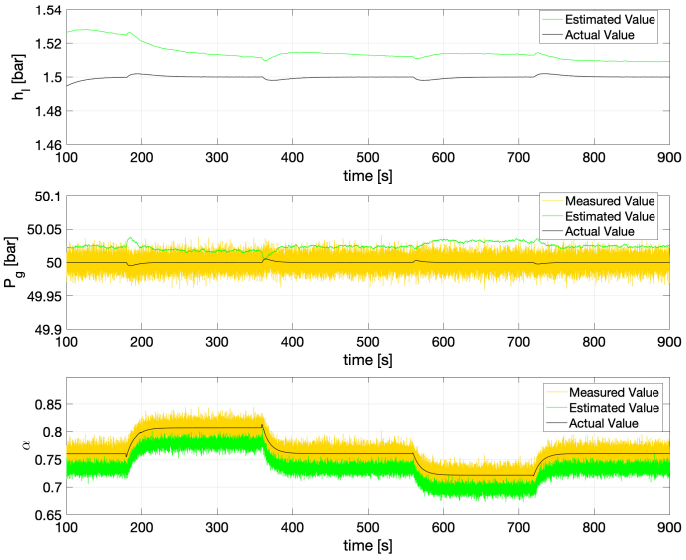

Fig. 5. EKF 100–900 s.

measurements of the liquid level are difficult and expensive to obtain; here the level estimated using other measurements. The simulation shows promising results, as the estimator model is a simplified model of the plant model, there is a plant-model mismatch, and this is reflected as bias in the estimated values.

In all cases, the UKF outperformed the EKF, as expected. A constrained UKF was used in this paper, where estimates outside of the feasible region were projected back to the feasible region. This is not an optimal way of solving the divergence problem that occurred in the UKF simulations, further investigation needs to be done on better methods to handle constraints in the states.

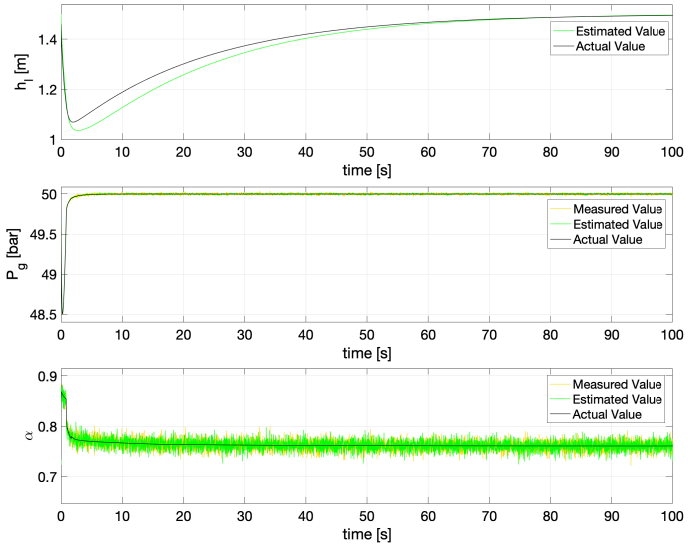

Fig. 6. UKF 0–100 s.

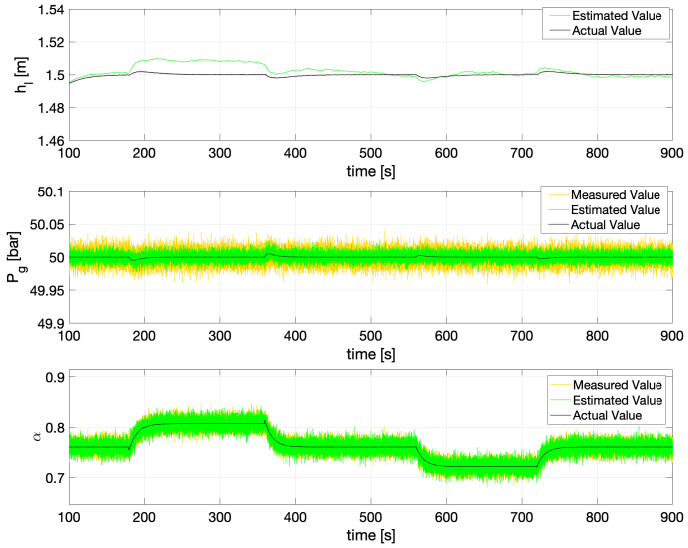

Fig. 7. UKF 100–900 s.

ACKNOWLEDGMENTS

This project is supported by the Norwegian Research Council, industrial partners and NTNU under the Subsea Production and Processing (SUBPRO) SFI program.

REFERENCES

[1] G. E. Kouba, O. Shoham, and S. Shirazi, "Design and performance of gas-liquid cylindrical cyclone separators," in *Proceedings of the BHR Group 7th International Meeting on Multiphase Flow., Cannes, France*, 1995, pp. 307–327.

[2] G. Kouba and O. Shoham, "A review of gas-liquid cylindrical cyclone (glcc) technology."

[3] S. Wang, R. Mohan, O. Shoham, G. Kouba *et al.*, "Dynamic simulation and control system design for gas-liquid cylindrical cyclone separators," in *SPE Annual Technical Conference and Exhibition*. Society of Petroleum Engineers, 1998.

TABLE III
PARAMETERS USED FOR SIMULATION

A	0.127 m^2
H	3.5 m
R	8.31434 Pa m^3
T	303 K
M_g	0.0240 Kg/mol
$\mathcal{T}$	2.2
ρ_l	857 Kg/m^3
ρ_g	43.2 Kg/m^3
C_{dl}	1
C_{dg}	1
A_{vl}	0.0324 m^2
A_{vg}	0.0324 m^2
P_{gb}	48 bar
P_{lb}	48 bar

[4] S. Wang, R. Mohan, O. Shoham, J. Marrelli, G. Kouba *et al.*, "Optimal control strategy and experimental investigation of gas-liquid compact separators," in *SPE Annual Technical Conference and Exhibition*. Society of Petroleum Engineers, 2000.

[5] M. Leskens, A. Huesman, S. Belfroid, P. Verbeek, A. Fuenmayor, P. Van den Hof, E. Nennie, and R. Henkes, "Fast model based approximation of the closed-loop performance limits of gas/liquid inline separators for accelerated design," *IFAC Proceedings Volumes*, vol. 44, no. 1, pp. 12 307–12 312, 2011.

[6] T. T. Kristoffersen, C. Holden, S. Skogestad, and O. Egeland, "Control-oriented modelling of gas-liquid cylindrical cyclones," in *American Control Conference (ACC),*, 2017, pp. 2829–2836.

[7] T. T. Kristoffersen and C. Holden, "Nonlinear model predicitve control of a gas-liquid cylindrical cyclone," in *25th Mediterranean Conference on Control and Automation (MED)*, 2017, pp. 66–73.

[8] ——, "Model predictive control and extended Kalman filter for a gas-liquid cylindrical cyclone," in *Control Technology and Applications (CCTA),*, 2017, pp. 1248–1255.

[9] ——, "State and parameter estimation for a gas-liquid cylindrical cyclone," in *European Control Conference(ECC)*, 2018.

[10] D. Simon, *Optimal state: Kalman H infinity and nonlinear approaches*. John Wiley and Sons, 2006.

[11] S. J. Julier and J. K. Uhlmann, "New extension of the kalman filter to nonlinear systems," in *Signal processing, sensor fusion, and target recognition VI*, vol. 3068. International Society for Optics and Photonics, 1997, pp. 182–194.

[12] ——, "Unscented filtering and nonlinear estimation," *Proceedings of the IEEE*, vol. 92, no. 3, pp. 401–422, 2004.

[13] R. G. Brown and P. Y. Hwang, *Introduction to random signals and applied kalman filtering: with matlab exercises and solutions,*, 4th ed. John Wiley & Sons, 2012.

[14] S. Sarkka, "On unscented Kalman filtering for state estimation of continuous-time nonlinear systems," *IEEE Transactions on automatic control*, vol. 52, no. 9, pp. 1631–1641, 2007.

[15] R. Kandepu, B. Foss, and L. Imsland, "Applying the unscented Kalman filter for nonlinear state estimation," *Journal of process control*, vol. 18, no. 7-8, pp. 753–768, 2008.

[16] D. Simon and T. L. Chia, "Kalman filtering with state equality constraints," *IEEE transactions on Aerospace and Electronic Systems*, vol. 38, no. 1, pp. 128–136, 2002.